



DIE ERDE

Journal of the
Geographical Society
of Berlin

The urban heat island of Basel – seen from different perspectives

Eberhard Parlow¹, Roland Vogt¹, Christian Feigenwinter¹

¹ Meteorology, Climatology and Remote Sensing, Department of Environmental Sciences, University of Basel, Klingelbergstr. 27, 4056 Basel, Switzerland, eberhard.parlow@unibas.ch, roland.vogt@unibas.ch, christian.feigenwinter@unibas.ch

Manuscript submitted: 15 July 2013 / Accepted for publication: 18 January 2014 / Published online: 2 September 2014

Abstract

For decades thermal infrared satellite imagery has been used for climate studies of a variety of geosystems, including urban areas. Additionally, airborne thermal remotely sensed data can provide high resolution information about urban land surface temperatures (LST). Numerous studies make use of these data for the investigation of urban-rural LST differences, commonly known as the urban heat island (UHI) phenomenon. Most of these studies try to analyse the urban heat island by means of the LST distribution. It seems that the UHI is easy to measure, easy to explain, easy to find, and easy to illustrate. Due to this apparent simplicity some people seem to jump into UHI studies without fully understanding the nature of the phenomenon as far as time and spatial scales, physical processes and the numerous methodological pitfalls inherent to UHI studies are concerned. In this study the use of thermal infrared satellite data with respect to the assessment of the surface UHI is investigated. The need to clearly distinguish between different types of UHI is emphasised by recalling the (surface) temperature and the UHI terminology. The pretended simplicity of UHI effects is in reality a result of complex interactions between local radiation conditions, earth surface heat budget, the urban structure and the boundary layer atmosphere. Different methods may provide completely different results. This paper aims to bring more clearness into the subject by assessing the urban heat island of the city of Basel, Switzerland, by the use of thermal data provided by satellites (Landsat TM/ETM+), helicopter-borne infrared camera (InfraTec VarioCAM®) and ground-based measurements of air temperature profiles. It is shown that UHIs vary essentially with the choice of the respective temperature (LST, air temperature) and height (surface level, street/canopy level, roof level).

Zusammenfassung

Die Auswertung von satellitengestützten Thermal-Infrarot-Bildern wird seit Jahrzehnten für Klimastudien verschiedener Ökosysteme genutzt, u.a. auch in Städten. Zusätzlich liefern Thermal-Befliegungen hochaufgelöste Informationen über Oberflächentemperaturen. Zahlreiche Studien nützen solche Daten für die Untersuchung von Temperatur-Differenzen zwischen städtischen und ländlichen Oberflächen, auch bekannt als städtischer Wärmeinseleffekt. In den meisten Studien wird der Wärmeinseleffekt anhand der räumlichen Verteilung der Oberflächentemperaturen analysiert. Dadurch entsteht der Eindruck, als sei der Wärmeinseleffekt einfach zu messen, einfach zu dokumentieren und unschwer zu erklären. Oftmals werden aber die grundlegenden physikalischen Prozesse bezüglich räumlicher und zeitlicher Skalen nicht berücksichtigt und viele Studien beinhalten methodische Ungenauigkeiten. Die vorliegende Studie untersucht den Gebrauch von Thermal-Infrarot-Satellitendaten im Hinblick auf die Bewertung des städtischen Wärmeinseleffekts. Die Notwendigkeit einer klaren Unterscheidung zwischen verschiedenen Wärmeinsel-Typen wird anhand der Terminologie für (Oberflächen-)Temperaturen und des Begriffs „Wärmeinsel“ aufgezeigt. Die vermeintliche Einfachheit des

Parlow, Eberhard, Roland Vogt and Christian Feigenwinter 2014: The urban heat island of Basel – seen from different perspectives. – DIE ERDE 145 (1-2): 96-110



DOI: 10.12854/erde-145-8

Wärmeinseleffekts ist in Wirklichkeit ein komplexes Zusammenspiel zwischen den lokalen Strahlungseigenschaften, dem Wärmehaushalt der Erdoberfläche, den urbanen Strukturen und der atmosphärischen Grenzschicht. Verschiedene Methoden liefern völlig verschiedene Resultate. Die vorliegende Studie hat zum Ziel, in dieser Hinsicht Klarheit zu schaffen. Dazu wird der Wärmeinseleffekt der Stadt Basel auf der Grundlage von Thermaldaten von Landsat TM/ETM+, einer Helikopter-Befliegung mit einer Infrarot-Kamera (InfraTec VarioCAM®) und von bodennahen vertikalen Profilen der Lufttemperatur untersucht. Es zeigt sich, dass der Wärmeinseleffekt erheblich von der verwendeten Temperatur (Luft- oder Oberflächentemperatur) und der betrachteten Höhe (Oberfläche, Strassen-/Bestandesniveau, Dachniveau) abhängt.

Keywords Urban heat island, urban surface heat island, thermal remote sensing

1. Introduction

Urbanisation is one of the most evident outcomes of human activities on climate. Meteorological variables like temperature, wind, humidity, heat stress, air pollution and many more are influenced. Fundamental differences of urban to non-urban conditions exist; namely the urban area

- has a high aerodynamic surface roughness which influences the vertical turbulence and wind field,
- has a completely different radiation and heat budget due to the physical and thermal properties of construction materials,
- is highly three-dimensional and therefore a very complex surface for all exchange processes within the urban boundary layer,
- is a significant source of emissions of greenhouse gases, pollutants and heat.

The most prominent feature of urban climate is the urban heat island (UHI) effect. The urban air temperature is generally some degrees higher than in the rural surroundings. UHIs can be found in most cities of the world, also smaller cities with populations less than 100 k are affected (Torok et al. 2001). The heat island intensity, i.e. the magnitude of the temperature difference (ΔT), correlates positively with the size of the town; there are, however, differences between European, North-American and Asian cities (Oke 1987) due to varying climate and topography, different distance to ocean or lake coast, different economic development, different construction types of buildings and diverse use of air conditioning in private and public houses, amongst others. However, with increasing number of UHI studies, the term “Urban Heat Island” is used for different phenomena which may

lead to confusion and misunderstanding. It is therefore essential that UHI studies clearly state which kind of heat island is addressed and what the underlying mechanisms are (Oke 1982, Roth et al. 1989). Voogt and Oke (2003) essentially distinguish between the atmospheric urban heat island (UHI) and the surface urban heat island (SUHI). The first mainly relies on ground-based in-situ measurements of air temperature and can be considered the classical way of assessing the UHI. This kind of UHI was first observed in the early 19th century by Luke Howard in London (see 1.2). Today, two kinds of atmospheric heat islands are addressed, depending on the observation height. Most commonly observed is the canopy layer urban heat island which relies on air temperature observations at street level. Measurements from urban flux towers, normally located on the roof of a building and already measuring properties of the urban roughness sub-layer, rather relate to the boundary layer urban heat island. On the other hand, SUHIs are observed by thermal remote sensors. The remote sensing approach to study the urban climate relies on thermal infrared data. Urban surfaces often show higher temperatures compared to their rural surroundings. Even if this effect is sometimes interpreted as the UHI effect, this well documented feature should be named Surface Urban Heat Island (SUHI) effect because the satellite sensor “sees” the long-wave emission or the surface temperature, respectively, and not the air temperature. The air temperature does not necessarily follow the spatial pattern of surface temperatures (Parlow 2011). Mean daily or annual urban air temperatures are generally some degrees higher than in the rural surroundings. This is a characteristic feature of the urban climate which can be found in most cities of the world. It is not limited to summer conditions only. If the diurnal course of air temperature differences between urban and rural sites are analysed, significant differences between day- and nighttime conditions can be found. Depending on the resolution

of the thermal infrared sensor, SUHIs may also be distinguished according to the level of the surface under consideration, i.e. street level or roof level. A very important question in remotely sensed thermal infrared imagery of urban areas is: “Where does the signal come from?” The urban surface is extremely complex and 3-dimensional. The medium resolution satellite sensors with grid sizes of 60 to 120 m integrate the signal over 3,600-14,400 m² which means that a single satellite pixel contains information from different land-cover types (roofs, streets, urban green space, water bodies etc.). This must always be kept in mind when thermal infrared satellite data are interpreted.

1.2 Background

The term “Urban Heat Island” goes back to the early 19th century. In 1820 *Luke Howard* (1772-1864), a pioneer of urban climatology, published “The Climate of London” in which he analysed air temperature measurements from the City of London and its rural surroundings (*Howard* 1833; republished by the International Association for urban climate (IAUC) in 2006). *Howard* discovered that during nighttime air temperatures were higher in London compared to the rural sites and that during daytime it was just the opposite. First remote sensing studies go back to the year 1972 (*Rao* 1972). While at the beginning the temperatures were compared to external land-use data, soon the derivation of land-use classes through multispectral imagery was possible. *Nichol* (1998), *Gallo and Owen* (1998), *Tal* (2001), and *Dousset and Gourmelon* (2003) used multispectral techniques to perform land-use or land-cover assessments from satellite data acquired at the same time as the thermal imagery. *Aniello et al.* (1995) used Landsat TM data to map micro-urban heat islands. *Quattrochi and Ridd* (1994) and *Voogt and Oke* (2002) used remote sensing data to analyse urban thermal properties. *Streutker* (2003) described urban heat islands in Houston/Texas. Increasing sensor resolution allows extracting temperatures from specific urban surfaces for analysis (*Quattrochi and Ridd* 1994). During the ESCOMPTE project in southern France three different multispectral satellite sensors were used to map the heat island of Marseille and some surrounding cities (*Mestayer et al.* 2005). During the Joint URBAN 2003 Tracer Field Experiment conducted in Oklahoma City (*Allwine et al.* 2004) field measurements on an instrumented van on routes through Oklahoma City and the rural outskirts were taken. In addition to this, ASTER surface kinetic temperatures of Oklahoma

City were analysed for six different land-use classes. The urban classes showed warmer daily surface temperatures than rural classes (*Brown et al.* 2004). During recent years analysis of SUHI has been repeated in many cities like Hamburg (*Bechtel* 2011), Beijing (*Cai et al.* 2011), Rome and Madrid (*Fabrizi et al.* 2010, 2011), Toulouse (*Houeta and Pigeon* 2011), 38 cities in the USA (*Imhoff et al.* 2010), Shanghai (*Li et al.* 2009) and many others. In most of these papers the surface urban heat island (SUHI) is analysed and most of the authors suggest that the surface temperature pattern is highly correlated to the air temperature without cross-checking with ground-based measurements to support this assumption. For further reading *Weng* (2009) gives an excellent review of current methods in thermal infrared remote sensing in the context of urban climate studies. More general reviews of UHI literature can be found in *Oke* (1982) and in *Arnfield* (2003).

In this paper the urban heat island of Basel, Switzerland, is analysed using three different data sets and thus relating to three different types of heat island. The SUHI is addressed comparing LST from a daytime and a nighttime Landsat-TM scene with a resolution of 60 and 120 m, respectively. The much higher resolution of 1 m LST from a helicopter-borne thermal infrared camera allows investigating the differences between street level and roof level SUHI. Finally, the UHI is investigated using ground-based air temperature and profile measurements from urban, sub-urban and rural sites. In the following section the data and methods are described and in *Section 3* the results are discussed with focus on the different perspectives of the evaluated heat islands.

2. Data and methods

2.1 Thermal infrared data (space-borne, Landsat TM/ETM+)

For the assessment of the SUHI from space two Landsat scenes, a daytime image and a nighttime image were analysed. The daytime scene was captured on August 12, 2000, 10:07 UTC, by Landsat 7 ETM+ and the night-time scene originates from Landsat 5 TM captured on August 29, 1999, 20:44 UTC. At-sensor brightness temperatures (i.e. the LST obtained on the satellite by TIR sensor) are calculated from Band 6 of the TM/ETM+ using the standard method (*Chander et al.* 2009) assuming that the earth’s surface is a black body with a spectral emissivity of 1, but including atmospheric effects (absorption and emissions along path).

Note that TM/ETM+ TIR sensors have different resolutions (120 m and 60 m, respectively) and the nighttime TM scene is affected by stripes. Because our analysis is mainly qualitative, the different resolutions and the stripes will not affect the interpretation.

2.2 High-resolution thermal infrared data (helicopter-borne)

High-resolution TIR data were recorded on July 1, 2009, between 13:00 and 14:00 CET by a helicopter-borne Infrared camera (InfraTec VarioCam®). The raw data were corrected for emissivity derived from literature values for urban surface materials. Urban surface materials were derived from imaging spectroscopy (APEX hyperspectral sensor) obtained during the HyperSwissNet flight campaign in July 2010. The final LST product with a 1 x 1 m² resolution was manually mosaicked and geo-rectified from more than 4000 single images recorded with a 1 Hz frequency during the flight and combined with information from a high-resolution 3D city model to account for urban morphology (e.g. height, slope and aspect of roofs). For more details refer to Koetz et al. (2009), Feigenwinter et al. (2011, 2012a), Jehle et al.

(2010) and the HyperSwissNet website (<https://hyperswissnet.wiki.geo.uzh.ch/Project>).

2.3 Ground-based air temperature and temperature profiles

Ground based measurements were carried out in and around the city of Basel over many years during various urban climate projects, especially the Regional Climate Project (REKLIP) (Parlow 1996), the Basel Urban Climate Project (BASTA) (Feigenwinter et al. 1999) and the Basel Urban Boundary Layer Experiment (BUBBLE) (Rotach et al. 2005). A unique data set is available from vertical profile measurements on a flux tower based on the roof of the institute from 1994 to 2003 (Basel Spalenring, BSPA). These measurements were continued with an extended setup after dislocation of the institute to Basel Klingelbergstrasse (BKLI) since 2003 to date. Vogt and Reber (1992), Feigenwinter et al. (1999), Christen and Vogt (2004), Rotach et al. (2005), Vogt and Parlow (2011) and Lietzke and Vogt (2013) give more details about the technical specifications of the sites and the technical equipment used. The locations and instrumentation used in this study are listed in Table 1.

Tab. 1 Summary of locations and measurement heights. Air temperatures were always measured using ventilated psychrometers except at the site Grenzach. z_H = mean building height, noV = no vegetation. wV = with vegetation (trees)

Location	Acronym	Height a.s.l. (m)	Coordinates	Land cover	Heights of measurements (m)	Data period
Spalenring 145	BSPA	278	47°33'17.6"N 07°34'34.6"E	Urban, dense, wV built-up, z _H =18 m	3, 4, 15.8, 22.9, 27.8, 32.9	1994-2003
Sperrstrasse 10	BSPR	255	47°33'57.2"N 07°35'48.8"E	Urban, dense, noV built-up, z _H =15 m	2.6, 14, 17.5, 21.5, 25.5, 31	2001-2002
Klingelbergstrasse 27	BKLI	265	47°33'42"N 7°34'50.7"E	Urban, dense, wV built-up, z _H =19 m	3, 6, 19	2003-
Lange Erlen	BLER	275	47°35'32.3"N 07°38'56.9"E	Rural, grassland	2, 5, 10	1990-
Fischingen	FISG	264	47°38'51"N 07°35'50"E	Rural, agricultural	2, 3, 5, 8, 10	1994-1995
Village Neuf	VLNF	240	47°37'7.6"N 07°33'27.1"E	Rural, agricultural	2	2002
Grenzach	GRNZ	265	47°32'12.0"N 07°40'31.5"E	Rural, grassland	1.5	2002

2.4 LST Terminology

In this section the terminology of LST as used in this paper is shortly revisited relying mainly on *Norman and Becker (1995)*, because terms like “canopy temperature”, “surface temperature”, “skin temperature”, etc. are widely used in the literature without further clarification.

Brightness temperature is the LST obtained from TIR sensors at satellite level assuming that the earth’s surface is a black body with emissivity 1, i.e. by the inversion of Planck’s law. This term is used in this paper for LST derived from Landsat data.

Directional radiometric surface temperature is the LST sensed on or immediately above the ground, reflecting the emissivity of each horizontal layer in the FOV of the radiometer. The radiometric temperature is dependent on the zenith view of the radiometer. If the sensed surface area is not homogeneous, the term ensemble directional radiometric surface temperature is appropriate. In this paper the term radiometric temperature is used for LSTs derived from helicopter-borne infrared camera, as this temperature may also refer to the hemispherical radiometric temperature as defined in *Norman and Becker (1995)*.

Canopy temperature is a non-specific term referring to the LST of the elements that form the canopy, i.e. trees and buildings (roofs) in the case of urban ecosystems. Depending on the resolution of the TIR sensor, brightness temperatures may partially include canopy temperatures.

Surface temperature is a general, non-specific term referring to the temperature of all objects comprising the area of the surface under consideration.

Skin temperature, though not used in this study, is a non-specific term that may refer to brightness temperature or radiometric temperature.

2.5 Heat island derivation

The Urban Heat Island is characterised by higher air temperatures inside the city at street level, which cannot be directly deduced from surface temperatures as seen by an airborne or space-borne sensor. It is therefore important that the fundamental underlying processes are considered. In fact, it is necessary to take the whole energy balance into account to make a con-

clusion about the urban climate and the pattern and intensity of the urban heat island.

Fundamental to urban radiation and energy balance are the following equations:

$$Q^* - (R_{sd} - R_{su} + R_{ld} - R_{lu}) = 0, \quad (1),$$

where net all-wave radiation Q^* is the sum of longwave and shortwave radiation fluxes R_{sd} , R_{su} , R_{ld} and R_{lu} , the shortwave (s)/longwave (l) downward (d)/upward (u) radiation, respectively, and

$$Q^* - (Q_H + Q_E + Q_S + Q_F) = 0, \quad (2),$$

where Q^* is partitioned into the latent heat flux Q_E , the sensible heat flux Q_H , the ground/storage heat flux Q_S , and the anthropogenic heat flux Q_F .

The terms of the urban radiation and energy budgets as formulated in *Eqs. 1* and *2* can be assessed in different ways. The most common method is by micrometeorological means. Q^* can be measured by net radiometers, more detailed information about its longwave/shortwave components may be obtained by installing upward/downward looking pyranometers (shortwave) and pyrgeometers (longwave). While the sensible and latent heat flux Q_H and Q_E can be directly measured by the eddy covariance method (*Feigenwinter et al. 2012b*) or profile and bulk methods (e.g. *Stull 1988*), Q_S and Q_F are mostly estimated by indirect methods because they are difficult, if not impossible, to measure. A popular method for the estimation of the storage term is the Objective Hysteresis Model (OHM) approach which relates Q_S (as the residual of *Eq. 2*) to Q^* and its first derivative (*Grimmond and Oke 1999*, *Rigo and Parlow 2007*). Q_F , being normally the smallest energy flux in *Eq. 2*, is mostly neglected or sometimes modelled (e.g. *Smith et al. 2009*). Numerous studies on urban climate made use of this micrometeorological approach (e.g. *Christen et al. 2003*, *Christen and Vogt 2004*, *Mestayer et al. 2005*, *Grimmond et al. 2004*, *Spronken-Smith et al. 2006*, *Frey et al. 2011*).

Ground-based in-situ measurements with a high temporal resolution as described above are indispensable for the validation of remote-sensing approaches for the estimation of urban radiation and heat fluxes. The combination of the two methods however provides the possibility to extend the limited spatial information of the micrometeorological measurements to a larger area covered by the remote sensor. Several studies successfully applied this combined methodologies.

In this study we applied a simple but robust method to derive the upwelling radiation fluxes in Eq. 1 from thermal infrared data using the ground-based radiation measurements of the incoming radiation fluxes R_{sd} and R_{ld} at the time of the overflight of the respective sensor. This approach assumes that R_{sd} and R_{ld} measured at one point are the same and valid for the whole area under consideration, being aware that there may be a larger deviation especially in the case of the Landsat scenes due to topography. Urban morphology (i.e. slope and aspect of roofs, shadows, sky view factor) was taken into account for the high-resolution scene. Broadband albedo was calculated by the formula provided by Liang (2001) for the Landsat scenes and the algorithm from Gruber et al. (2003) for spectral to broadband albedo conversion for the high-resolution scene taking into account different weighting functions for diffuse and direct radiation according to in-situ measurements at the time of the overflight. Outgoing shortwave radiation is then calculated as αR_{sd} , with α as the respective broadband albedo. Outgoing longwave radiation R_{lu} is computed according to the Stefan-Boltzmann law:

$$R_{lu} = \varepsilon \sigma LST^4 \quad (3),$$

with ε as the emissivity and σ the Stefan-Boltzmann constant ($5.67 \times 10^{-8} \text{ W m}^{-2} \text{ K}^{-4}$). Emissivity ε is assumed to be 1 for the Landsat scenes. For the high resolution scene ε was derived from literature values for urban surface materials (see also section 2.2) and the sky view factor was considered.

The simplified approach for the Landsat scenes was previously applied by Parlow (2000, 2003), who investigated short and longwave radiation fluxes and the net radiation from satellite data for Basel using Landsat data. Chrysoulakis (2003) used ASTER data to calculate the net radiation of Athens. Frey et al. (2007) also determined with ASTER data the radiation fluxes and budget of Dubai and Abu Dhabi. For the megacity of Cairo the full radiation balance and heat fluxes were computed using ASTER satellite imagery (Frey et al. 2011, Frey and Parlow 2012).

A major problem in the estimation of turbulent heat fluxes using thermal satellite imagery lays in the difference between the observed brightness temperature of the surface and the required aerodynamic temperature (Norman and Becker 1995, Mahrt et al. 1997), which relates the brightness temperature to the efficiency of heat exchange between the surface

and the overlaying atmosphere and thus drives the sensible heat transfer (Kustas et al. 2007). The brightness temperature depends on the sensor's field of view (FOV) and, therefore, the complex 3D-geometry of roofs, walls and buildings of urban environments has to be taken into account. The parameterisation of the geometry of urban canyons remains a crucial problem in this field of research, especially when working with satellite data whose spatial resolution stays below the size of buildings. According to Voogt and Oke (2003) the use of sensor view models helps to deepen the understanding of the relation between urban surfaces and satellite imagery. Sensor view models represent the buildings as block-like elements on a plane surface and provide only crude approximations of the actual complexity of urban surfaces. A detailed investigation on the influence of the 3D-geometry of urban structures on spatially distributed radiation fluxes was published by Frey and Parlow (2008).

The determination of the urban surface radiation balance or the heat fluxes encounters several difficulties because of the inhomogeneous surface in urban areas. According to Nunez and Oke (1977), Arnfield (1982) and Arnfield and Grimmond (1998) the storage heat flux depends on surface albedo and surface material properties. Detailed analysis was carried out on the storage heat flux, which is of prominent importance in urban environments and makes up to 30-50 % of the daytime net radiation, by Rigo and Parlow (2007). The urban energy balance and therefore the storage flux are influenced strongly by the surface radiation fluxes of urban canyons.

3. Results

In the following three different approaches for the assessment of the urban heat island of Basel are compared referring to the data sets introduced in the previous section.

3.1 Landsat thermal infrared imagery

Figure 1 shows the typical distribution of brightness temperatures of the city of Basel at daytime (Fig. 1a) and nighttime (Fig. 1b). In both examples the city of Basel centred in the image has higher brightness temperatures compared to the non-urban surroundings. The airport in the northwest as well as industrialised areas differ by 5-10 K from the rural surfaces. Due to

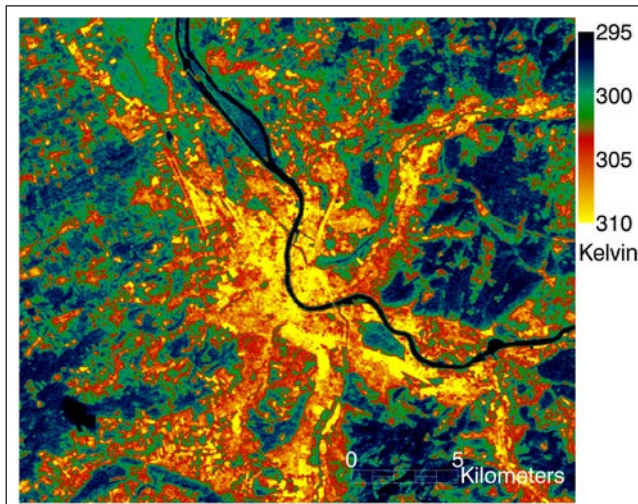


Fig. 1a Landsat-7-ETM+ thermal infrared, 12 Aug. 2000, 11:07 local time (CET), 60 m resolution resampled to 30 m resolution grid

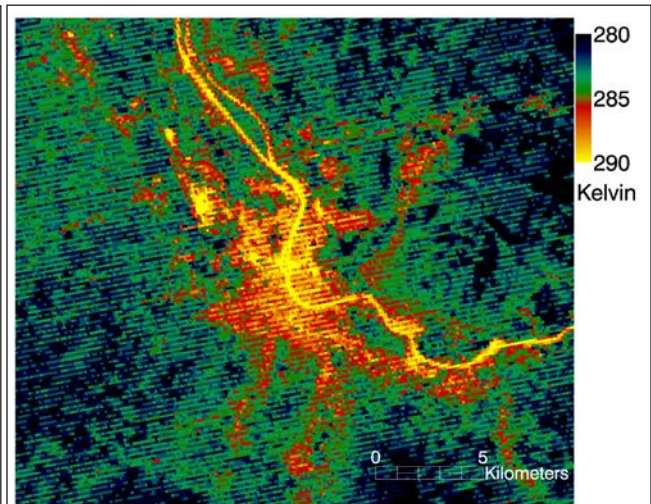


Fig. 1b Landsat-5-TM thermal infrared, 29 Aug. 1999, 21:44 CET, 120 m resolution resampled to 30 m resolution grid

the extreme heat capacity of water the temperatures of the River Rhine, bending through the city centre, are coldest during daytime but warmest during nighttime relative to land surface conditions. The high daytime brightness temperatures are related to the surface albedo and the thermal properties of the surface materials, i.e. heat conductivity and heat capacity. All surfaces have a positive net radiation (Fig. 2) during daytime in the range between about 400 Wm^{-2} (e.g. airport (high albedo and high brightness temperatures)) and 500 Wm^{-2} (e.g. residential areas (medium albedo and brightness temperatures)) with a maximum of about 600 Wm^{-2} of the water surfaces of River Rhine (lowest albedo and lowest brightness temperatures). Topographic effects are visible in the southern and north-eastern hills surrounding the city with high net radiation on the south-eastern slopes due to higher incoming shortwave radiation, low surface temperatures and low albedo of the dominating forest land cover. In the absence of topography, i.e. in the closer city surroundings, and in the industrial regions in the north-west the warmer surfaces generally correspond to lower net radiation during daytime. Note that in contrast to Figure 1a the city is not the same eye catcher anymore in the net radiation image (Fig. 2). In the night scene from 1999 the range of brightness temperatures is smaller and the spatial distribution is smoother which is a common feature at that time of day and a result of the coarser grid size of 120 m because a single pixel integrates over an area of $14,400 \text{ m}^2$. The striping of the image originates from noise of the satellite sensor and was not corrected for this study.

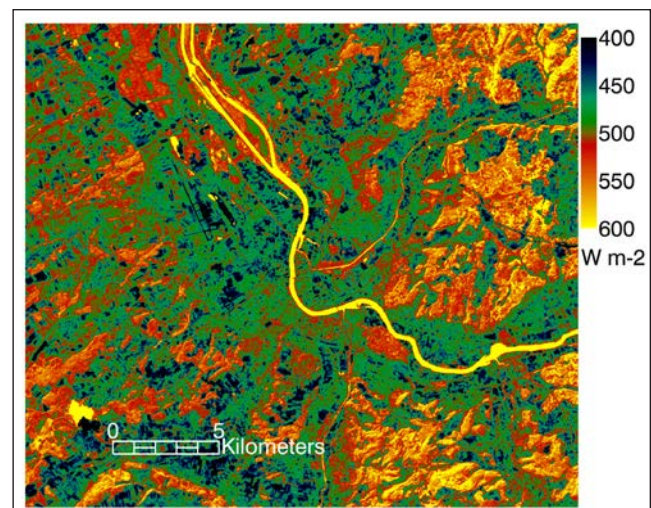


Fig. 2 Net radiation derived from Landsat-7-ETM+ thermal infrared and incoming radiation measurements during satellite overpass from ground-based station BSPA, 12 Aug. 2000, 11:07 CET, 60 m resolution resampled to 30 m resolution grid

During nighttime all surfaces have a negative net radiation in the range of -10 to -70 Wm^{-2} , which can be derived from Figure 1b assuming uniform incoming longwave radiation of 338 Wm^{-2} as measured during satellite overflight at the ground-based station BSPA and an emissivity Eq. 1. The most negative values correspond with those pixels which show highest surface temperatures. Due to the absence of shortwave radiation fluxes the radiation and heat balance in Eqs. 1 and 2 simplifies to:

$$R_{ld} - R_{lu} = Q_H + Q_E + Q_S + Q_F$$

The high brightness temperatures of impervious urban surfaces are a feature that holds during the whole night, which means that the negative net radiation must be balanced by the heat fluxes. The prime candidate for this compensation is the storage heat flux Q_s which during daytime gets up to 50 % of net radiation. This gain of heat during daytime is released during nighttime to efficiently and completely balance the energy loss through net radiation. Christen and Vogt (2004) showed that even during the night the direction of the sensible heat flux remains upward from the surface to the atmosphere and is therefore not contributing to the compensation of the negative net radiation. Therefore nocturnal temperatures in urban systems are not decreasing drastically and remain on a level several degrees higher when compared to rural air temperatures.

3.2 High-resolution thermal infrared imagery from helicopter measurements

A digital surface model of the city of Basel with a spatial resolution of 1 m was available providing additional information for the analysis of this high-resolution scene. Data hold the information of building height above ground level, including slope and aspect. Figure 3a shows this data layer with the River Rhine, the medieval city centre on the left side, the Swiss Railway Station at the bottom and highly industrialised city quarters and the German Railway Station on the top right edge. This data was used to

compute the percentages of roofs seen by a satellite sensor with a grid size of $60 \times 60 \text{ m}^2$ (Fig. 3b).

Three typical urban structures can be roughly separated using simple roof fractions: *i*) high-density built-up districts with clearly more than 50 % of roofs within a $60 \times 60 \text{ m}^2$ grid cell (region A (medieval town centre), region B (high-density residential and industrial area) and region C (Swiss Railway Station and connected industrial functions)), *ii*) medium-density residential areas with percentages between 25-40 % of roof influence (region D) and *iii*) urban green spaces with values close to 0 % (region E (Zoological Garden), region F (Schützenmattpark) and region G (Kannenfeldpark)). From this crude classification it is obvious that in most inner-city regions the satellite measurement of brightness temperatures is predominantly from roof level and therefore not correlated to air temperatures at screen level in 2 m above ground, the medium-density residential areas will be a mixture of both resulting in mixed brightness temperatures of roof and ground level. Also the signal from urban green spaces is not a pure ground-level signal as it also refers to canopy brightness temperatures from trees.

Figure 4a shows the radiative temperatures for the city centre. One can clearly distinguish between the roof level (mostly in orange/yellow) at about 311-318 K, the asphalt and concrete surfaces of streets at 306-311 K (red/orange) and the green spaces (parks and backyards) at 300-306 K (green). The River Rhine shows



Fig. 3a Buildings in Basel city centre (pixel size 1 m)

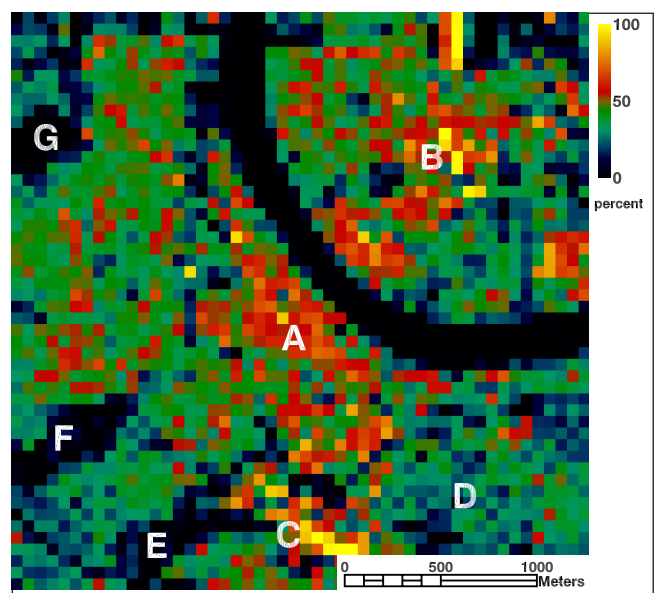


Fig. 3b Percentage of roofs in Basel city centre (pixel size 60 m)

The urban heat island of Basel – seen from different perspectives

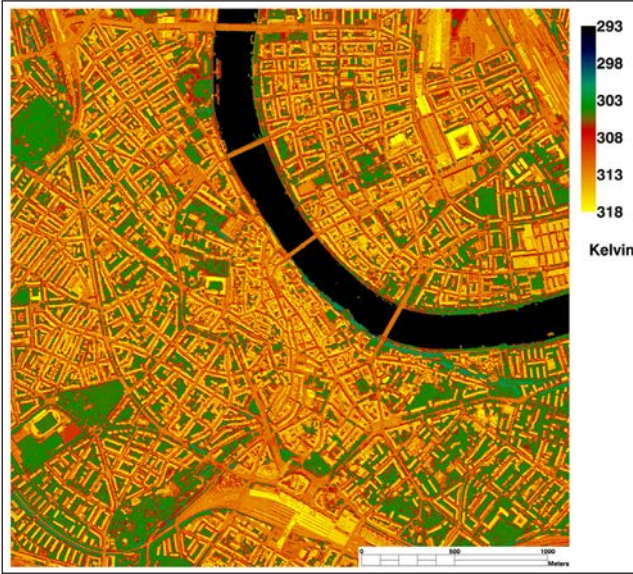


Fig. 4a Radiative temperatures of Basel city (pixel size 1 m) derived from helicopter-borne infrared camera

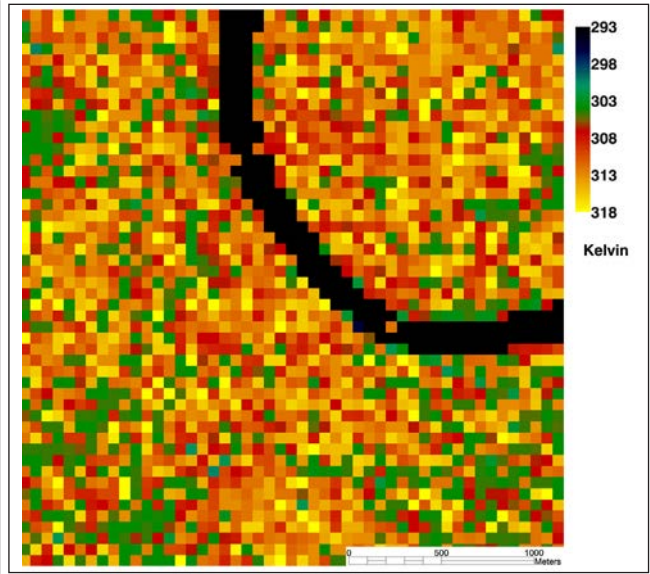


Fig. 4b Resampled radiative temperatures from Figure 4a to a pixel size of 60 m

a brightness temperature of 293 K. Statistics are given in Figure 5 as a histogram. Computed over all pixels the mean radiative temperature at roof level is 40.9 °C (314 K) with a standard deviation $\sigma = 2.7$ K, at ground level the mean radiative temperature is only 33.9 °C (307 K) with $\sigma = 5.1$ K. This difference between roof level and ground level corresponds to a difference in long-wave emission R_{lu} of about 50 Wm^{-2} (551 vs. 503 Wm^{-2}).

Figure 6 shows the net radiation as derived from high resolution LSTs in Figure 4a (see also sections 2.2 and 2.5) using the measurements from the Klingelbergstrasse flux tower for incoming shortwave and longwave fluxes. Land cover types that are very fragmented and small compared to the dominant ones have a decreasing influence when data are filtered and smoothed to coarser grid resolutions. Therefore increasing the

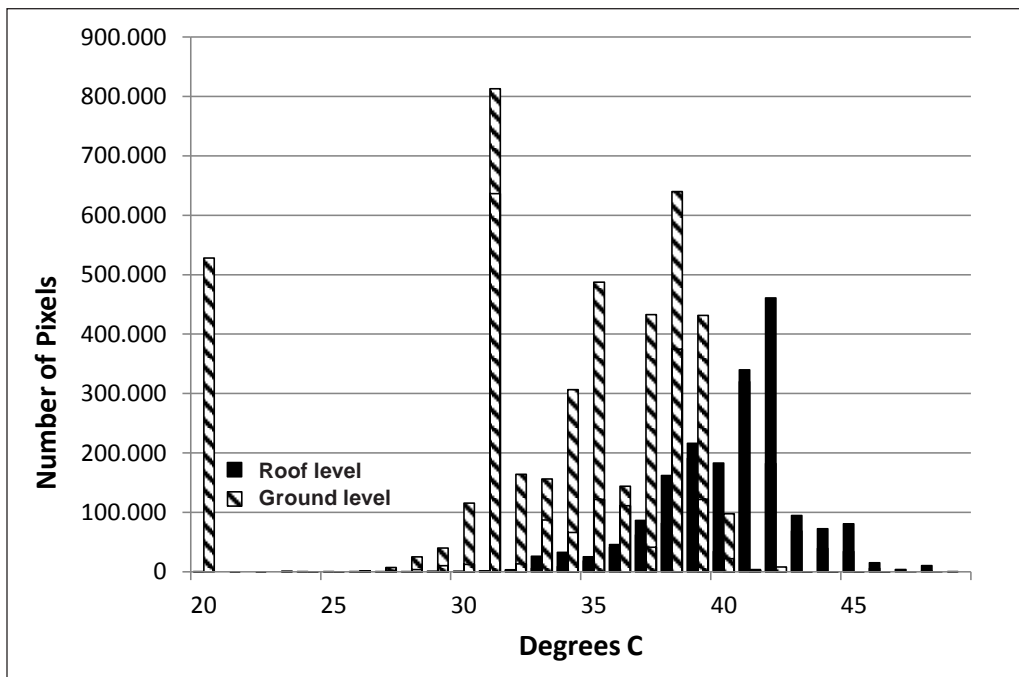


Fig. 5 Histogram of radiative temperatures at ground and roof level during helicopter flight campaign. Note the large part at 20 °C corresponds to water bodies.

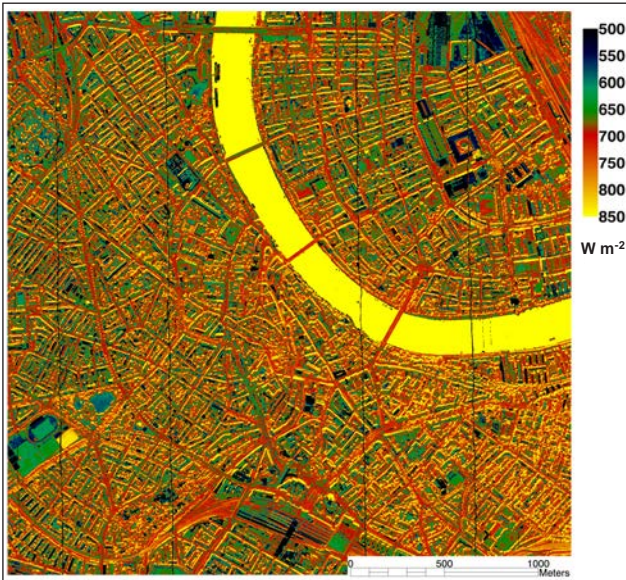


Fig. 6a Net radiation Q^* derived from LST in Fig. 4a and albedo values from Fig. 6b (see Sections 2.2 and 2.5). Vertical stripes result from pixel columns used for APEX sensor calibration.

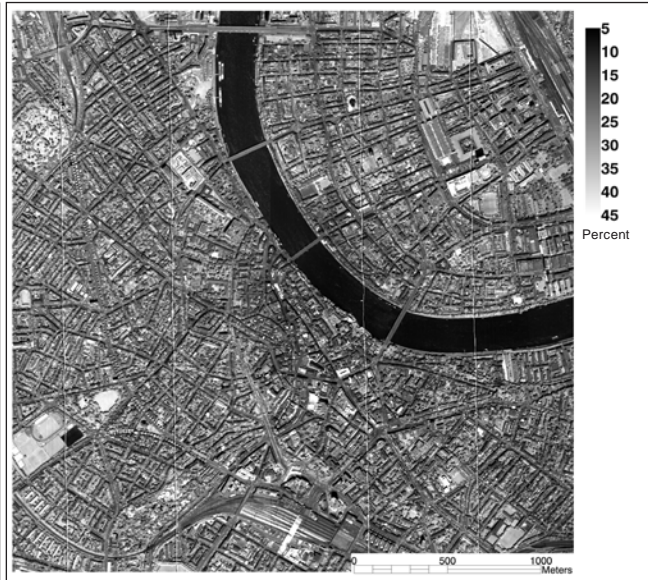


Fig. 6b Broadband albedo as derived from hyperspectral data during HyperSwissNet campaign in July 2010 (see Sections 2.2 and 2.5)

pixel size from $1 \times 1 \text{ m}^2$ to $60 \times 60 \text{ m}^2$ simulates what a satellite sensor like Landsat would have measured. The result is shown in Figure 4b. As expected a large part of the city is dominated by pixels with high surface temperatures influenced by the high percentages of roofs in the designated pixel. Only larger urban green spaces keep their original lower temperature level. No significant correlation of sky-view factors based on the 1-m-digital surface model was found neither for roof surface temperatures nor ground level temperatures.

3.3. Time-series analysis of temperature measurements at different heights above ground

In the following section the temporal courses of the UHI of Basel, i.e. air temperature differences between urban and rural locations, are analysed. Figure 7 shows the differences between the urban site Basel-Spalenring (BSPA, 3 m above ground) and the rural site Lange Erlen (BLER, 2 m above ground) as mean hourly values between 1994 and 2003. At the top the mean daily and running daily means over these 10 years are displayed. At the bottom the isopleths are given in 0.25 K steps. Daily mean values range around +0.7 K during winter and have their maximum at the start of summer with +1.3 K. If no shorter time intervals are considered then Basel has a clear UHI all along the year. But in the bottom graph hourly mean temperature differences are

shown and one can clearly see that during daytime – when satellite thermal infrared imagery shows increased brightness/surface temperatures in the city – the air temperature differences over the whole year are very low and range from +0.25 to +0.5 K. This rapidly changes during the night, especially after sunset, when the UHI reaches maximum values of up to +2.5 K.

The frequency of the hourly UHI values shows that over the 10 years period 75 % of all hourly mean differences were in the range between -2 and 2 K, most of them with positive and a minority with negative deviations. 14 % range from 2 to 4 K, 9 % from 4 to 6 K and only 2 % have maximum deviations of 6 to 8 K. These situations are exclusively during nighttime and are correlated with high summer temperatures.

Since the human being lives in the urban canopy layer it is reasonable to compare measurements at the 2 m above ground level. However, as in dense urban areas most of the energy exchange between urban surface and boundary layer atmosphere takes place at roof level it is of interest to compare also above roof level with rural temperatures. Therefore in Figure 8 above-roof measurements of two urban stations are included and averaged diurnal courses of UHI of different urban-rural combinations are displayed.

Three groups of different temperature courses can be distinguished especially during the afternoon: the

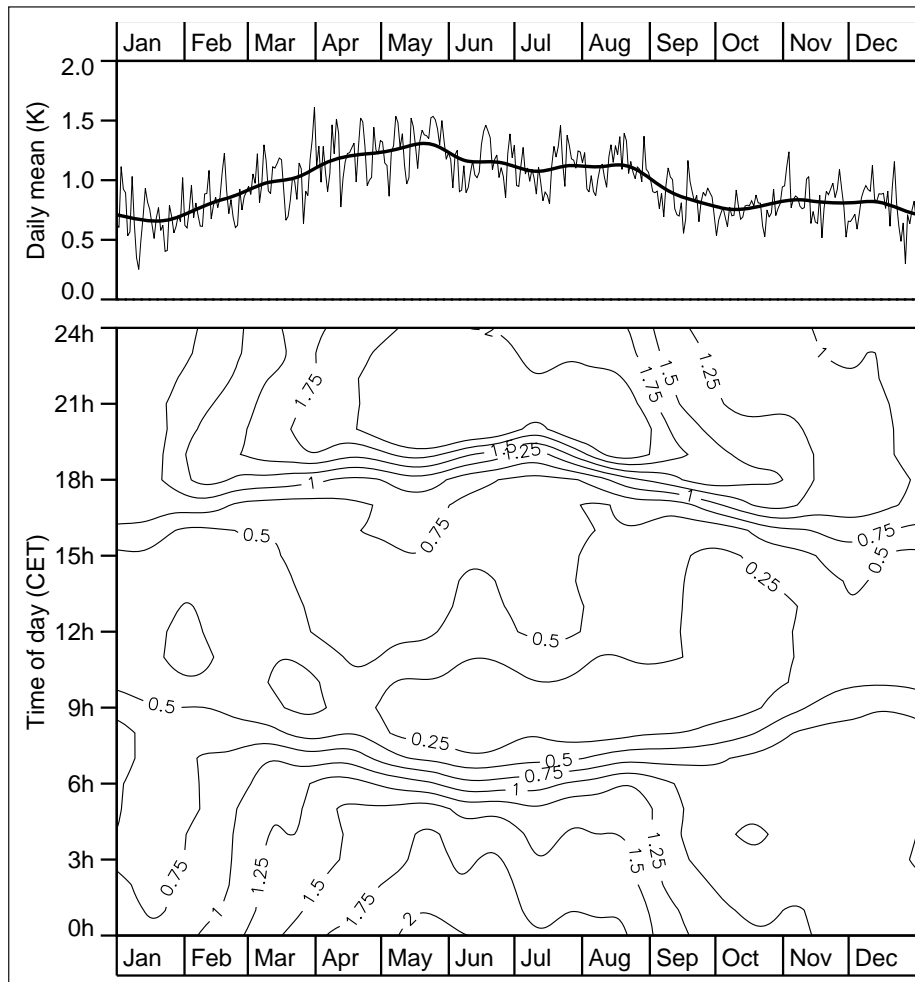


Fig. 7 Differences of air temperatures urban – rural between the stations Basel Spalenring (3 m, street) and Lange Erlen (2 m, grassland) based on hourly mean values for 1994 – 2003. Top: Mean daily and daily running means. Bottom: Thermo-isopleths in 0.25 K steps.

“above roof” comparison (○, □), the urban-grassland comparison (▲, ●), and the urban-agricultural comparison (■, ◆). Of special interest is the above-roof comparison because the UHI is slightly reduced during the night compared to the 2 m above ground levels and during daytime both urban stations show a well-developed urban cooling island effect. This has also been demonstrated over longer time periods of several years (Parlow 2011). This is at the first glance surprising since the mean roof surface temperatures are 7 K warmer, as shown in Figures 4 and 5. But if the complete energy budget is considered it becomes clear that high absorption of energy by the storage heat flux during daytime limits the sensible heat flux, and surface temperature and air temperature at the same height above ground are mostly decoupled. All stations show a higher UHI effect during the first half of the night. The urban-agricultural comparison has an intermediate position. The reason might be that the agricultural

crop has mostly been harvested during the time period resulting in a different heat budget behaviour. In the case of Grenzach (▲) another reason could be that at this station no ventilated psychrometers were used which can result in an offset of temperature measurements of 1 K during daytime. The different temperatures at the urban stations at ground level can be explained with the alley trees at Spalenring (BSPA) and no vegetation at Sperrstrasse (BSPR).

4. Discussion

Among the numerous factors influencing the urban heat island effect (UHI) are external drivers like geographical latitude, topography or distance to the open sea as well as local drivers like albedo, imperviousness, building height, vegetation ratio and, in part, the thermal properties of the surface material. These

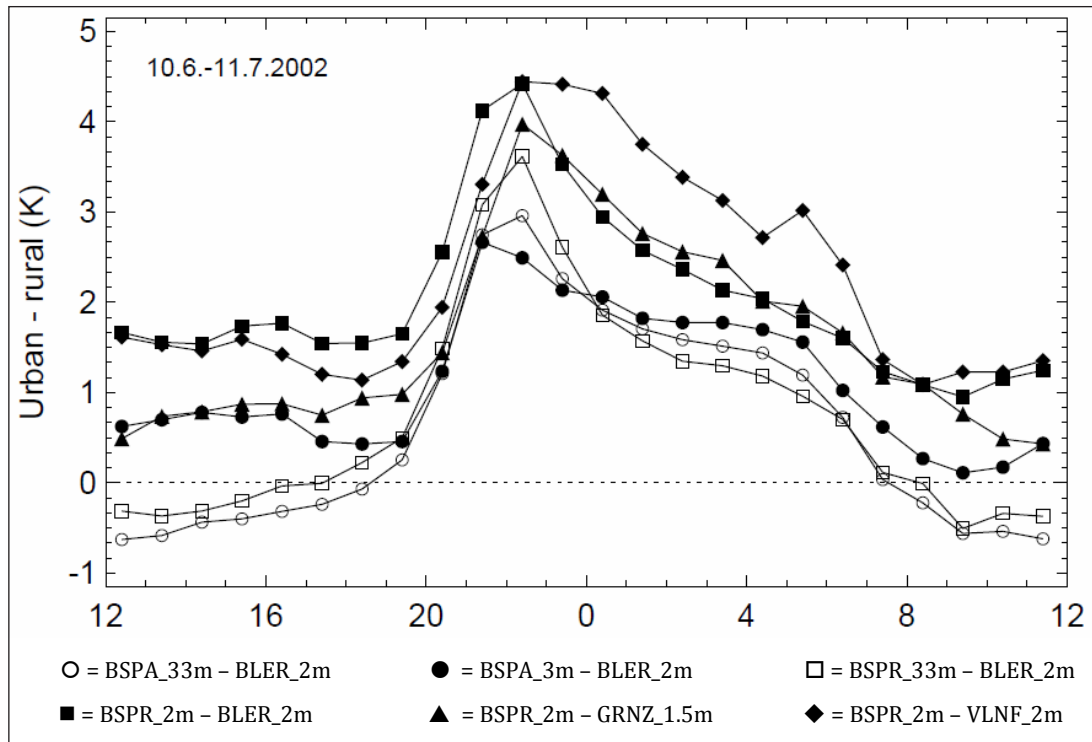


Fig. 8 Mean diurnal courses of UHI between the urban stations Basel-Spalen-ring (BSPA) or Basel-Sperrstrasse (BSPPR) and the rural stations Lange Erlen (BLER), Grenzach (GRNZ) or Village Neuf (VLNF). Note that midnight is centred on the X-axis. For further information about measurement locations and instrumentation refer to Table 1. (CET = Central European Time)

properties, i.e. heat capacity and heat conductivity, mainly rule the local storage heat flux which is the major variable for the UHI. During daytime up to 30-50 % of the net radiation is used for the storage flux which automatically limits the sensible heat flux since net radiation is quite similar at rural and urban sites. Due to the large urban storage heat flux the available energy for the two turbulent heat fluxes (sensible and latent) is reduced. During the night this absorbed energy is released and used to compensate the nocturnal negative net radiation at the urban site mostly completely (Christen and Vogt 2004) preventing the air temperatures to decline to low values like at rural sites.

The result of any UHI investigation strongly depends on the origin of the specific temperature used for the analysis. It is shown in this study that urban heat islands have to be defined according to the layer for which the derived temperature is valid. We showed an example for a surface urban heat island SUHI, which results from the analysis of brightness temperatures derived from Landsat TM/ETM+ data. With a resolution of 120 m and 60 m, respectively, the value of a single pixel represents in most cases a mixture of street level and roof level brightness temperature. In the core

of a city, the roof level fraction dominates as these are highly built-up areas and therefore, the SUHIs derived from Landsat TM/ETM+ rather refer to roof level. The nighttime scene highlights the impervious surfaces as the hot spots of the nocturnal SUHI. The daytime SUHI in the late morning is only weakly developed.

A higher resolution, i.e. 1 x 1 m² pixel size, and radiative temperatures measured with a helicopter-borne infrared camera allow, in combination with a 3D building model, to separate roof-level from street-level SUHIs. It is shown that the street-level SUHI is rather a cooling island while the roof-level SUHI is similar to the one derived from coarser resolution satellite data, but is more intensive at this time of day (i.e. around solar zenith). The regression of radiative temperatures with the sky-view factors from ground level and roof level revealed no significant correlation, respectively.

The most classical way for the estimation of UHI intensity is by means of air temperature measurements. But also in this case the location and height of the measurement are essential. Canopy layer UHIs can be derived from street canyon measurements, while the intensity of boundary layer UHIs can be evaluated from temperature measurement at a flux tower.

5. Conclusions

The simple approach to use thermal infrared satellite data only to prove the existence of a canopy layer urban heat island is mostly wrong. Firstly, since satellite data are mostly captured during daytime satellite passes when the urban heat island is not well-developed, secondly, since most of the satellite measurements represent roof level brightness temperatures of the cities and this surface temperature is mostly decoupled from the air temperatures at the same level. In most cases there is an urban cooling island at roof level when compared with rural air temperature conditions near the ground.

In any case it is highly recommended to use the right terms when results of UHI or SUHI studies are published.

Acknowledgements

The authors acknowledge the financial support from projects HyperSwissNet (Schweizerische Universitätskonferenz SUK) and GEOURBAN (S&T Cooperation Program Switzerland-Russia in the framework of the ERA.Net-RUS Program). The comments of the reviewers are highly acknowledged.

References

- Allwine, K.J., K. Clawson, M.J. Leach, D. Burrows, R. Wayson, J. Flaherty and E. Allwine 2004: Urban dispersion processes investigated during the Joint Urban 2003 Study in Oklahoma City. – 5th AMS Conference on Urban Environment, 26 August 2004, Vancouver, B.C.
- Aniello, C., K. Morgan, A. Busbey and L. Newland 1995: Mapping micro-urban heat islands using Landsat TM and GIS. – *Computers and Geosciences* **21** (8): 965-969
- Arnfield, A.J. 1982: An approach to the estimation of the surface radiative properties and radiation budgets of cities. – *Physical Geography* **3**: 97-122
- Arnfield, A.J. 2003: Two decades of urban climate research: A review of turbulence, exchanges of energy and water, and the urban heat island. – *International Journal of Climatology* **23**: 1-26
- Arnfield, A.J. and C.S.B. Grimmond 1998: An urban canyon energy budget model and its application to urban storage heat flux modelling. – *Energy and Buildings* **27** (1): 61-68
- Bechtel, B. 2011: Multitemporal Landsat data for urban heat island assessment and classification of local climate zones. – In: *Stilla, U., P. Gamba, C. Juergens, D. Maktav* (eds.): Joint Urban Remote Sensing Event. – Munich: 129-132
- Brown, M.J., A. Ivey, T.N. McPherson, D. Boswell and E.R. Pardyjak 2004: A study of the Oklahoma City urban heat island using ground measurements and remote sensing. – 5th AMS Conference on Urban Environment, 26 August 2004, Vancouver, B.C.
- Cai, G., M. Du and Y. Xue 2011: Monitoring of urban heat island effect in Beijing combining ASTER and TM data. – *International Journal of Remote Sensing* **32** (5): 1213-1232
- Chander, G., B.L. Markham and D. Helder 2009: Summary of current radiometric calibration coefficients for Landsat MSS, TM, ETM+, and EO-1 ALI sensors. – *Remote Sensing of Environment* **113**: 893-903
- Christen, A. and R. Vogt 2004: Energy and radiation balance of a central European city. – *International Journal of Climatology* **24** (11): 1395-1421
- Christen, A., C. Bernhofer, E. Parlow, M.W. Rotach and R. Vogt 2003: Partitioning of turbulent fluxes over different urban surfaces. – 5th International Conference on Urban Climate, 1-5. September 2003, Lodz, Poland
- Chrysoulakis, N. 2003: Estimation of the all-wave urban surface radiation balance by use of ASTER multispectral imagery and in-situ spatial data. – *Journal of Geophysical Research* **108** (D18): 4582
- Dousset, B. and F. Gourmelon 2003: Satellite multi-sensor analysis of urban surface temperatures and landcover. – *Journal of Photogrammetry and Remote Sensing* **58** (1-2): 43-54
- Fabrizi, R., A. de Santis and A. Gomez 2011: Satellite and ground-based sensors for the urban heat island analysis in the city of Madrid. – In: *Stilla, U., P. Gamba, C. Juergens, D. Maktav* (eds.): Joint Urban Remote Sensing Event. – Munich: 349-352
- Fabrizi, R., S. Bonafoni and R. Biondi 2010: Satellite and ground-based sensors for the urban heat island analysis in the city of Rome. – *Remote Sensing* **2** (5): 1400-1415
- Feigenwinter, C., R. Vogt and E. Parlow 1999: Vertical structure of selected turbulence characteristics above an urban canopy. – *Theoretical and Applied Climatology* **62**: 51-63
- Feigenwinter, C., E. Parlow and A. Damm 2011: Radiative and derived thermal properties of urban surface materials using APEX imaging spectroscopy data. – Karlsruhe Institute of Technology (KIT), International Conference on Climate and Construction, Karlsruhe, Germany, 24-25 October 2010
- Feigenwinter, C., E. Parlow and A. Damm 2012a: Urban sub-surface heat flux derived from APEX imaging spectroscopy data. – 8th International Conference of Urban Climate ICUC8, Dublin, Ireland, 6-10 August 2012
- Feigenwinter, C., R. Vogt and A. Christen 2012b: Eddy covariance measurements over urban areas. – In: *Aubinet, M., T. Vesala and D. Papale* (eds.): Eddy covariance. A practical guide to measurement and data analysis. – Dordrecht et al. : 377-397
- Frey, C.M., G. Rigo and E. Parlow 2007: Urban radiation balance of two coastal cities in a hot and dry environment. – *International Journal of Remote Sensing* **28** (12): 2695-2712

- Frey, C.M. and E. Parlow 2008: Geometry effect on the estimation of band reflectance in an urban area. – *Theoretical and Applied Climatology* **96**: 395-406
- Frey, C.M., E. Parlow, R. Vogt, M. Harhash and M. Abdel Wahab 2011: Flux measurements in Cairo. Part 1: In-situ measurements and their applicability for comparison with satellite data. – *International Journal of Climatology* **31** (2): 218-231
- Frey, C.M. and E. Parlow 2012: Flux Measurements in Cairo. Part 2: On the determination of the spatial radiation and energy balance using ASTER satellite data. – *Remote Sensing* **4** (9): 2635-2660
- Gallo, K.P. and T.W. Owen 1998: Assessment of urban heat islands: A multi sensor perspective for the Dallas-Ft. Worth, USA region. – *Geocarto International* **13**: 35-41
- Grimmond, C.S.B. and T.R. Oke 1999: Heat storage in urban areas: Local-scale observations and evaluation of a simple model. – *Journal of Applied Meteorology* **38**: 922-940
- Grimmond, C.S.B., J.A. Salmond, T.R. Oke, B. Offerle and A. Lemonsu 2004: Flux and turbulence measurements at a densely built-up site in Marseille: Heat, mass (water and carbon dioxide), and momentum. – *Journal of Geophysical Research: Atmospheres* **109** (D24): 27
- Gruber, S., D. Schlöpfer and M. Hoelzle 2003: Imaging spectrometry in high-alpine topography: the derivation of accurate broadband albedo. – 3rd EARSeL Workshop on Imaging Spectroscopy, Oberpfaffenhofen, Germany, 13-16 May 2003
- Houet, T. and G. Pigeon 2011: Mapping urban climate zones and quantifying climate behaviours – An application on Toulouse urban area (France). – *Environmental Pollution* **159** (8-9): 2180-2192
- Howard, L. (1833): *The Climate of London*. Vols. 1, 2, 3. – 2nd edition. – Reprint by the International Association for Urban Climate (IAUC) 2006. – London
- Imhoff, M.L., P. Zhang, R.E. Wolfe and L. Bounoua 2010: Remote sensing of the urban heat island effect across biomes in the continental USA. – *Remote Sensing of Environment* **114** (3): 504-513
- Jehle, M., A. Hueni, A. Damm, P. D'Odorico, J. Weyermann, M. Kneubühler, D. Schlöpfer, M.E. Schaepman and K. Meuleman 2010: APEX – current status, performance and validation concept. – *IEEE Sensors* 2010: 533-537. – DOI: 10.1109/ICSENS.2010.5690122
- Koetz, B., K. Itten, M. Borgeaud, D. Brunner, B. Buchmann, C. Feigenwinter, F. Hüsler, M. Kneubühler, E. Parlow, A. Psomas, S. Wunderle and N.E. Zimmermann 2009: HYPER-SWISS-NET: Fostering the Swiss research community in the field of imaging spectroscopy. – EARSeL Workshop on Imaging Spectrometry, Tel Aviv, Israel, 2009
- Kustas, W.P., M.C. Anderson, J.M. Norman and F. Li 2007: Utility of radiometric-aerodynamic temperature relations for heat flux estimation. – *Boundary-Layer Meteorology* **122** (1): 167-187
- Li, J.J., X. Wang, X. Wang, W. Ma and H. Zhang 2009: Remote sensing evaluation of urban heat island and its spatial pattern of the Shanghai metropolitan area, China. – *Ecological Complexity* **6** (4): 413-420
- Liang, S. 2001: Narrowband to broadband conversions of land surface albedo. I: Algorithms. – *Remote Sensing of Environment* **76** (2): 213-238
- Lietzke, B. and R. Vogt 2013: Variability of CO₂ concentrations and fluxes in and above an urban street canyon. – *Atmospheric Environment* **74**: 60-72
- Mahrt, L., J. Sun, J.I. MacPherson, N.O. Jensen and R.L. Desjardins 1997: Formulation of surface heat flux. Application to BOREAS. – *Journal of Geophysical Research: Atmospheres* **102** (D24): 29641-29649
- Mestayer, P.G., P. Durand, P. Augustin, S. Bastin, J.-M. Bonnefond, B. Bénech, B. Campistron, A. Coppalle, H. Delbarre, B. Dousset, P. Drobinski, A. Druilhet, E. Fréjafon, C.S.B. Grimmond, D. Groleau, M. Irvine, C. Kergomard, S. Kermadi, J.-P. Lagouarde, A. Lemonsu, F. Lohou, N. Long, V. Masson, C. Moppert, J. Noilhan, B. Offerle, T.R. Oke, G. Pigeon, V. Puygrenier, S. Roberts, J.-M. Rosant, F. Sanid, J. Salmond, M. Talbaut and J. Voogt 2005: The urban boundary-layer field campaign in Marseille (ubl/clu-escompte): Set-up and first results. – *Boundary-Layer Meteorology* **114** (2): 315-365
- Nichol, J.E. 1998: Visualisation of urban surface temperatures derived from satellite images. – *International Journal of Remote Sensing* **19** (9): 1639-1649
- Norman, J.M. and F. Becker 1995: Terminology in thermal infrared remote sensing of natural surfaces. – *Remote Sensing Reviews* **12** (3-4): 159-173
- Nunez, M. and T.R. Oke 1977: The energy balance of an urban canyon. – *Journal of Applied Meteorology* **16**: 11-19
- Oke, T.R. 1982: The energetic basis of the urban heat island. – *Quarterly Journal of the Royal Meteorological Society* **108** (455): 1-24
- Oke, T.R. 1987: *Boundary layer climates*. – 2nd edition. – London
- Parlow E. 1996: The regional climate project REKLIP – an overview. – *Theoretical and Applied Climatology* **53** (1-3): 3-7
- Parlow, E. 2000: Remotely-sensed heat fluxes of urban areas. – In: Dear, R.J., J.D. Kalma, T.R. Oke and A. Auliciems (eds.): *Biometeorology and urban climatology at the turn of the millennium*. Selected Papers from the Conference ICB-ICUC'99, Sydney, 8-12 Nov. 1999. – WMO Technical Documents **1026**. – Geneva: 523-528
- Parlow E. 2003: The urban heat budget derived from satellite data. – *Geographica Helvetica* **59**(2): 99-111
- Parlow, E. 2011: Urban climate. – In: Niemelä, J. (ed.): *Urban ecology. Patterns, processes, and applications*. – Oxford et al.: 31-44
- Rao, P.K. 1972: Remote sensing of urban heat islands from an environmental satellite. – *Bulletin of the American Meteorological Society* **53** (8): 647-648

- Rigo, G. and E. Parlow 2007: Modelling the ground heat flux of an urban area using remote sensing data. – *Theoretical and Applied Climatology* **90** (3-4): 185-199
- Rotach, M.W., R. Vogt, C. Bernhofer, E. Batchvarova, A. Christen, A. Clappier, B. Feddersen, S.-E. Gryning, G. Martucci, H. Mayer, V. Mitev, T.R. Oke, E. Parlow, H. Richner, M. Roth, Y.-A. Roulet, D. Ruffieux, J.A. Salmond, M. Schatzmann and J.A. Voogt 2005: BUBBLE – an urban boundary layer meteorology project. – *Theoretical and Applied Climatology* **81** (3-4): 231-261
- Roth, M., T.R. Oke and W.J. Emery 1989: Satellite-derived urban heat islands from three coastal cities and the utilization of such data in urban climatology. – *International Journal of Remote Sensing* **10** (11): 1699-1720
- Smith, C., S. Lindley and G. Levermore 2009: Estimating spatial and temporal patterns of urban anthropogenic heat fluxes for UK cities: the case of Manchester. – *Theoretical and Applied Climatology* **98** (1-2): 19-35
- Spronken-Smith, R. A., M. Kossmann and P. Zavar-Reza 2006: Where does all the energy go? Surface energy partitioning in suburban Christchurch under stable wintertime conditions. – *Theoretical and Applied Climatology* **84** (1-3): 137-149
- Streutker, D.R. 2003: Satellite-measured growth of the urban heat island of Houston, Texas. – *Remote Sensing of Environment* **85** (3): 282-289
- Stull, R.B. 1988: An introduction to boundary layer meteorology. – *Atmospheric Sciences Library* **13**. – Dordrecht et al.
- Tal, A. 2001: Surface temperatures and urban land-use from satellite imagery – the case of Tel Aviv-Jaffa. – In: Jürgens, C. (ed.): *Remote sensing of urban areas = Fernerkundung in urbanen Räumen*. Abstracts and full papers of the 2nd International Symposium held in Regensburg, Germany, June 22-23, 2001. – *Regensburger Geographische Schriften* **35**: 99 -100
- Torok, S.J., C.J.G. Morris, C. Skinner and N. Plummer 2001: Urban heat island features of southeast Australian towns. – *Australian Meteorological Magazine* **50** (1): 1-13
- Vogt, R. und S. Reber 1992: Das REKLIP-Energiebilanzmessnetz. Aufbau, Ausstattung, Test und erste Ergebnisse des Basler REKLIP-Messnetzes. – *Regio Basiliensis* **33** (2): 81-92
- Vogt, R. und E. Parlow 2011: Die städtische Wärmeinsel von Basel – tages- und jahreszeitliche Charakterisierung. – *Regio Basiliensis* **52** (1): 7-15
- Voogt, J.A. and T.R. Oke 2003: Thermal remote sensing of urban climates. – *Remote sensing of Environment* **86**: 370-384
- Voogt, J.A. and T.R. Oke 2002: Remote sensing and modelling of urban heat islands. – 4th Symposium on the Urban Environment, American Meteorological Society, 20-24 May 2002, Norfolk VA: 54-55
- Weng, Q. 2009: Thermal infrared remote sensing for urban climate and environmental studies: Methods, applications, and trends. – *ISPRS Journal of Photogrammetry and Remote Sensing* **64** (4): 335-344